Supporting Information

Sulfur-assisted ammonia treatment of fibrous carbon matrix to fabricate high-content pyrrole-type Fe-N-C catalyst for superior oxygen reduction

Hongyin Hu[a†], Rui Qiao[a†], Runyang Miao[a], Huimin Sun[a], Fang Duan[a], Han Zhu[a], Mingliang Du[a], Shuanglong Lu*[a]

a. Key Laboratory of Synthetic and Biological Colloids, Ministry of Education, School of Chemical and Material Engineering, Jiangnan University, Wuxi 214122, P. R. China.

† These authors contributed equally to this work.

*Correspondence: Email: lushuanglong@jiangnan.edu.cn (S. L.)

Contents

1. Experimental section

Reagents. 2-methylimidazole (98%), N,N-dimethylformamide (DMF, ≥99.5%), $ZnCl_2$ (Analytical Reagent (AR)), $Fe(NO_3)_3 \cdot 9H_2O$ (AR), ethanol (AR), isopropyl alcohol (AR) and sublimated sulfur() were purchased from Sinopharm Chemical Reagent Co., Ltd. Dicyandiamide (98%) was purchased from TCI (Shanghai) Development Co., Ltd. Polyacrylonitrile (PAN) with MW:150000 g mol^{-1} was purchased from Sigma-Aldrich. Argon (Ar, 99.999%) and ammonia (NH_3, 99.999%) were bought from Xinxiyi Technology Co., Ltd. Deionized water (resistivity: ca.18.42 MΩ cm) was used to prepare the electrolyte solutions. All reagents and solvents used in experiments were commercially available and were used without further purification.

Synthesis of PAN-Im fibers. Typically, PAN (1 g) and 2-methylimidazole was dissolved in 8.5 g DMF by magnetic stirring for 12 h under room temperature as the electrospinning solution. The resulting solution was transferred into a 10 mL syringe with a stainless-steel syringe needle. For the electrospinning process, a positive voltage of 10 kV was supplied to the needle. The feeding rate and distance between needle and collector of tinfoil were set at 0.6 mL h^{-1} and 14 cm, respectively. Then, the obtained electrospinning membrane was moved into a vacuum oven to remove the solvent at 60 ℃ for 12 h.

Synthesis of Zn-Im porous coordination polymer fibers. The PAN/Im fibers (100 mg) were added to ethanol (18 g) solution containing $ZnCl_2$ (50 mg) and reacted at 120 ℃ for 1 day to obtain brown PAN/Zn-Im fibers. Then it was washed three times with ethanol and DMF. Then transferred to flask and soaked with DMF under 60 ℃. Replaced the DMF per hours for a total of five times to remove PAN and obtained Zn-Im fibers. The prepared membrane was washed three times with ethanol and moved into a vacuum oven to remove the solvent at 40 ℃ for 6 h.

Synthesis of porous carbon fiber fibers. The Zn-Im fibers were pyrolyzed in a tube furnace at 900 ℃ at 5 ℃ min^{-1} and kept for 3 h under flowing argon atmosphere. Then, after the pyrolysis system was cooled to room temperature naturally. The product was then leached by refuxing in a 0.5 M H_2SO_4 solution for 18 h to effectively remove most of the coordinated Zn. The washed with deionized water until pH neutral and dried at 60 ℃ for 12 h.

Synthesis of Im-Fe-NS-900. First, ground the porous carbon fibers to powder-like. Next, 100 mg porous carbon fiber powder was dispersed into an isopropanol solution (50% v/v) containing 5.0 mg $Fe(NO_3)_3 \cdot 9H_2O$ and 10.0 mg cyanamide. After 1 h ultrasonication and 10 h magnetic stirring under 60℃, the Fe^{3+} and cyanamide adsorbed porous carbon fiber powder was collected by centrifugation and then dried at 60 °C. And the product was called Im-Fe^{3+}. 10 mg Im-Fe^{3+} was mixed with 100 mg sublimated sulfur and pyrolyzed in a tube furnace at 900 ℃ at 5 ℃ min^{-1} and kept for 2.5 h under flowing argon atmosphere and 0.5 h under flowing argon and ammonia mixed atmosphere (1:14, v/v). Then, after the pyrolysis system was cooled to room temperature naturally.

Im-Fe-900 were synthesized by a similar method except without sublimated sulfur and ammonia atmosphere.
Im-Fe-N-900 were synthesized by a similar method except without sublimated sulfur.

Im-Fe-S-900 were synthesized by a similar method except without ammonia atmosphere.
Im-Fe-NS-800 and Im-Fe-NS-1000 were synthesized by a similar method except pyrolysed under different temperate.
ZIF-8-Fe-NS-900 were synthesized by a similar method except change Zn-Im PCP fiber membrane with ZIF-8.

Characterizations. Field-emission scanning electron microscope (FE-SEM, Hitachi, Japan, S-4800) and transmission electron microscope (TEM, Hitachi, JEM-2100 plus) operated at an acceleration voltage of 3 kV and 200 kV were used to characterize the morphology, size and crystal structures of the samples.
The elemental mappings were recorded on scanning transmission electron microscope (STEM, acceleration voltage of 300 kV, Philips-FEI, Tecnai G2 F30S-Twin).
X-ray diffraction (XRD) patterns were acquired at a scanning rate of 0.02 2θ s^{-1} in the 2θ range of 10–90° using a Bruker AXS D8 Advance X-ray diffractometer with Cu Kα radiation (λ=0.15406 nm).
X-ray photoelectron spectroscopy was performed with a Thermo Scientific ESCALAB 250XI system.
Raman spectroscopy was measured with Horiba Scientific LabRAM HR Evolution with 532 nm.
Thermal gravity analysis (TGA) was recorded on NETZSCH STA 449 F5 from 30 to 900 °C at a heating rate of 10 °C min^{-1} under N_2 flow.

Electrochemical Measurements. The electrochemical tests of as-prepared catalysts were conducted in an Iviumatat electrochemical workstation. To prepare the catalyst ink, the catalyst (3 mg) was first dispersed in 970 μL isopropyl alcohol under sonication for 30 min, following which, 30 μL of 5 wt% Nafion solution was added into the above solution form a homogeneous ink. Then 20 μL catalyst ink was loaded onto the glassy carbon electrode (disk diameter, 5 mm; geometric area, 0.196 cm^2) to fabricate working electrode ($loading_{catalyst}$: 0.46 mg cm^{-2}).
The RDE system (Pine, USA) was used to evaluate the performance of the catalyst. The glassy carbon electrode coated with catalyst, carbon rod and $Hg/HgCl_2$ reference electrode were used as working electrode, counter electrode and reference electrode, respectively. The electrolyte is 0.1 M KOH solution. The mentioned potential was calibrated with respect to reversible hydrogen electrode (RHE) based on the following equation of $E_{(RHE)} = E_{(Hg/HgCl2)} + 0.244 + 0.0591pH$. The linear polarization curves were collected in saturated oxygen electrolyte at a scan rate of 10 mV s^{-1}. It is worth noting that the ORR polarization curves have been corrected in the N_2-saturated electrolyte to eliminate the interference of double layer capacity. The stability test was conducted by applying a constant voltage of 0.6 V vs. RHE in O_2-saturated basic solution.
Calculation of the yield of H_2O_2 and the electron transfer number (n) are illustrated as follows:

$$H_2O_2\% = \frac{I_R/N_0}{I_D + I_R/N_0} \times 200 \quad (1)$$

$$n = 4 \times \frac{I_D}{I_D + I_R/N_0} \quad (2)$$

where I_D represents the disk current, I_R represents the ring current, N_0 is the collection efficiency

of the RRDE (In this experiment is 0.37).

Besides, the electron transfer number can also be extracted from the Koutecky-Levich (K-L) equation:

$$\frac{1}{j} = \frac{1}{j_L} + \frac{1}{j_K} = \frac{1}{B\omega^{1/2}} + \frac{1}{j_K} \quad (3)$$

$$B = 0.62nFC_0D_0^{2/3}\upsilon^{-1/6} \quad (4)$$

in which j is the experimental current density, j_K is the kinetic current, C_0 is the bulk concentration of O_2 (1.2×10^{-6} mol cm^{-3}), D_0 is the diffusion coefficient of O_2 in 0.1 M KOH (1.9×10^{-5} cm^2 s^{-1}), F is the Faraday constant (96485 C mol^{-1}), υ is the kinetic viscosity (0.01cm^2 s^{-1}), and ω is the rotation speed (in radians per minute).

Zinc-air battery tests. The Zinc-air battery tests were performed in a home-made zinc-air cell, which was assembled with 6.0 M KOH and 0.2 M $Zn(Ac)_2$ as the electrolyte, the zinc plate as anode and the catalyst-loading carbon cloth as air cathode. The catalyst ink was prepared by dispersing 3 mg catalyst into 970 μL isopropyl alcohol and 30 μL of 5 wt% Nafion solution, followed by sonication for 60 minutes. Then 200 μL ink was loaded on the carbon paper as the cathode. All the battery tests were carried on a CHI 660D at the room temperature.

2. Supporting Figures

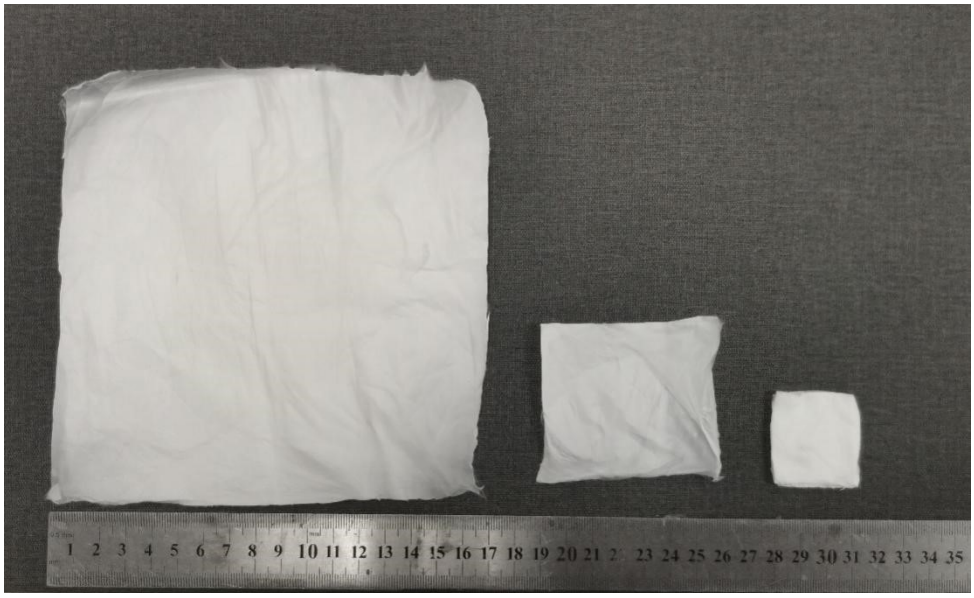

Figure S1. Photograph of Im-PAN fibrous membrane.

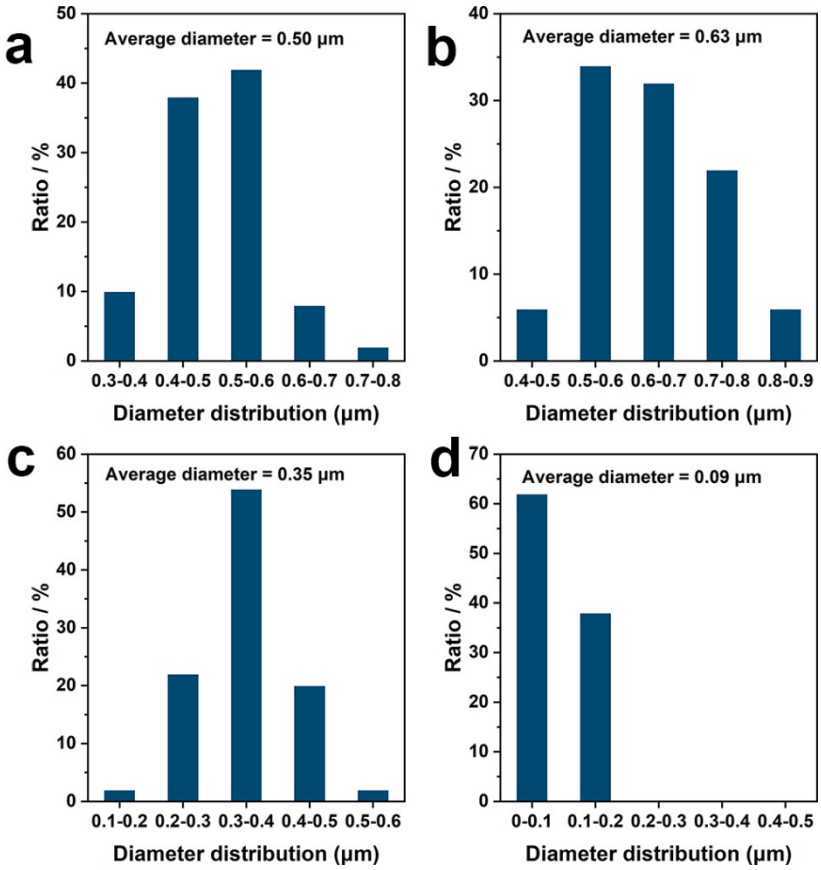

Figure S2. The diameter distribution of fibers. (a) Im/PAN fibers; (b) Zn-Im/PAN fibers; (c) Zn-Im fibers; (d) Zn-Im derived porous carbon fibers.

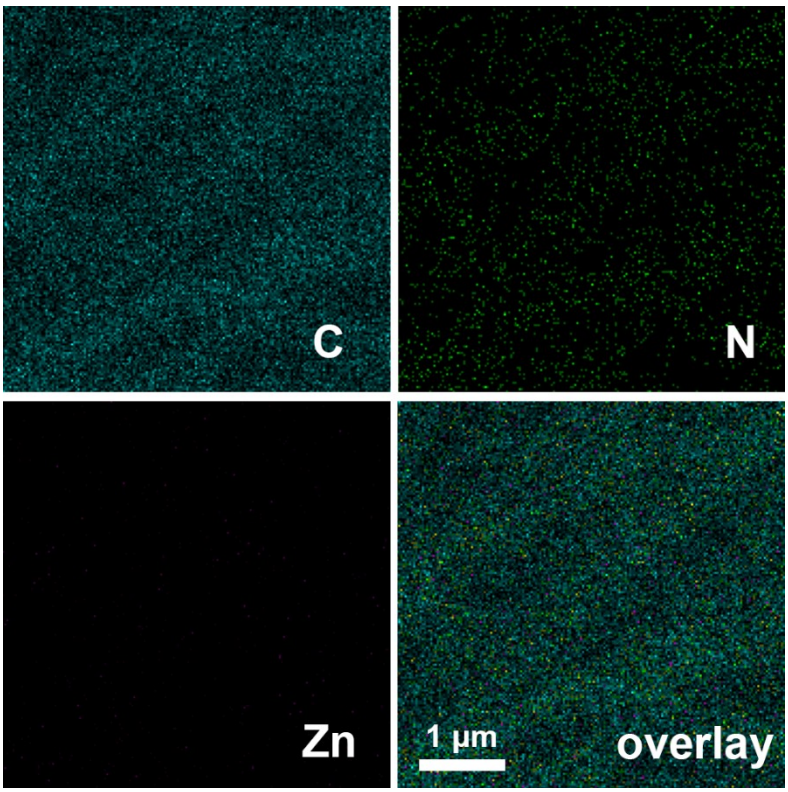

Figure S3. SEM-EDS mapping spectrum of PAN/Im fibers.

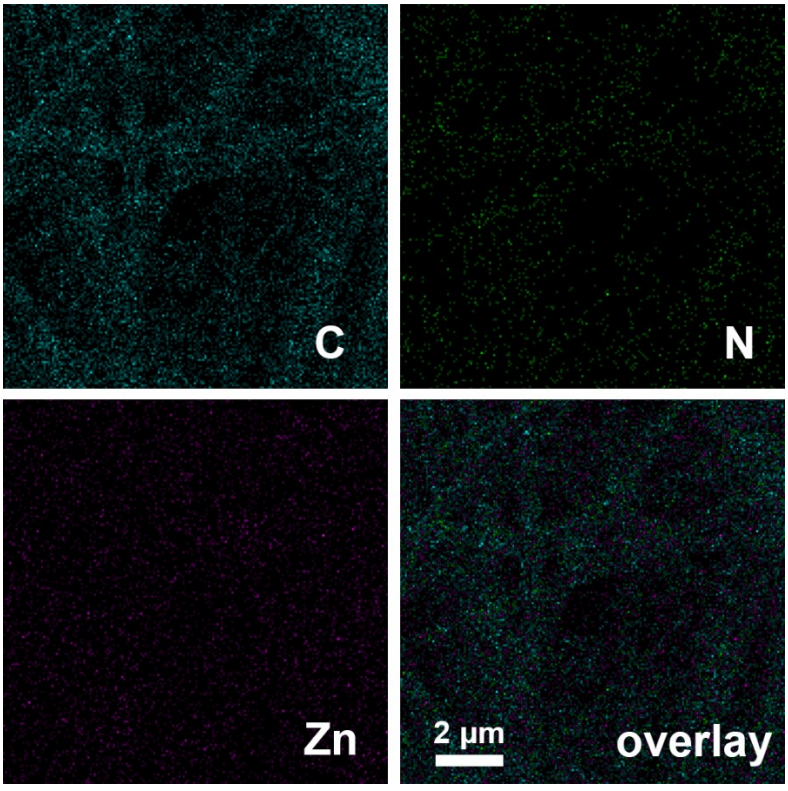

Figure S4. SEM-EDS mapping spectrum of PAN/Zn-Im fibers.

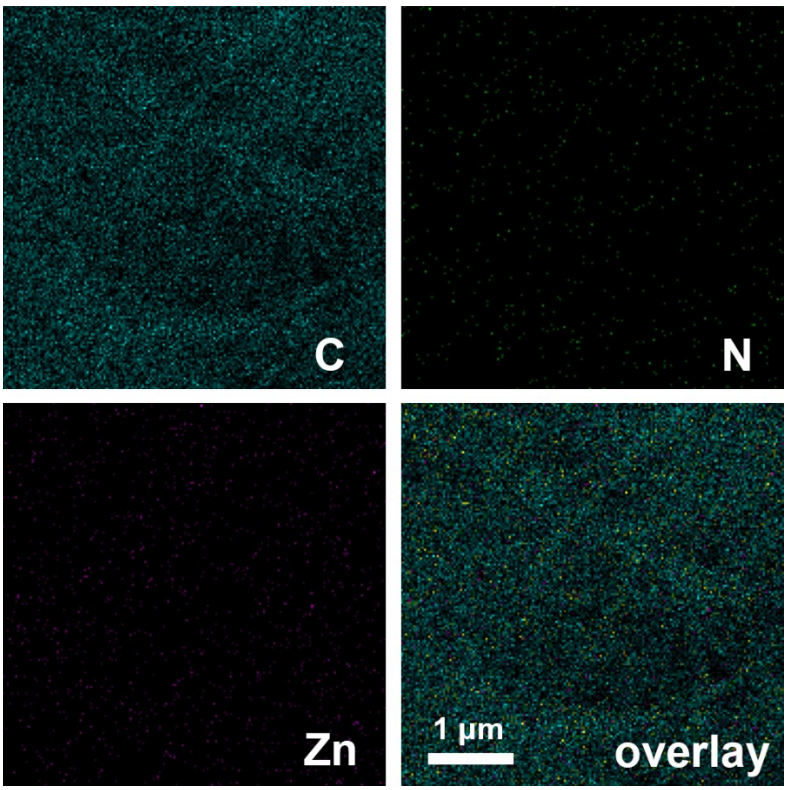

Figure S5. SEM-EDS mapping spectrum of porous carbon fibers.

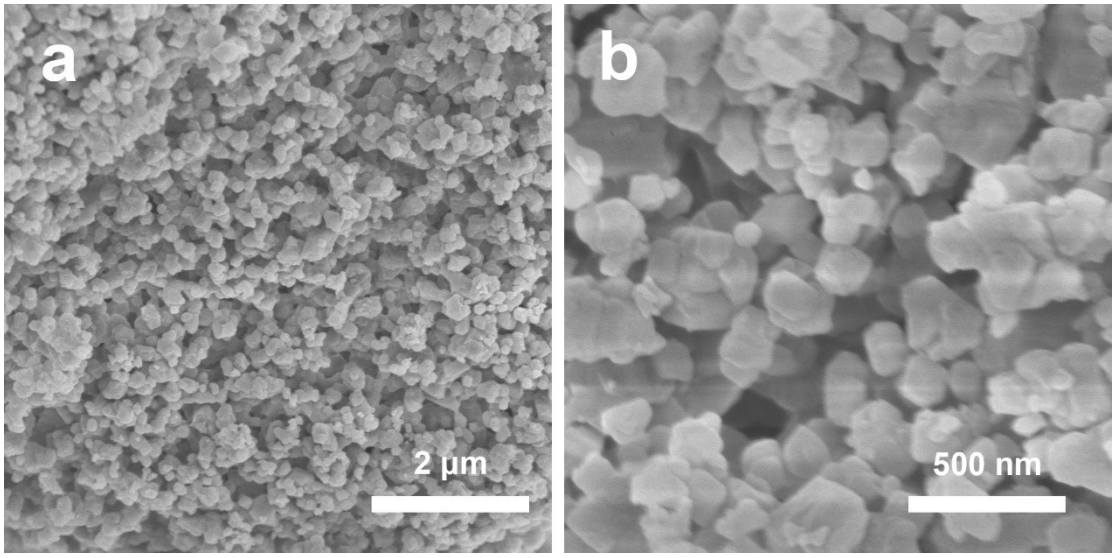

Figure S6. SEM images of ZIF-8 nanoparticles.

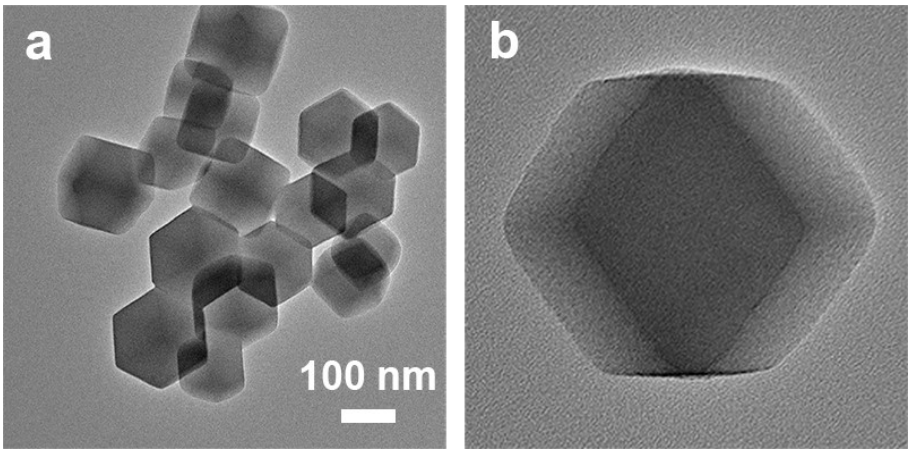

Figure S7. TEM images of ZIF-8 nanoparticles.

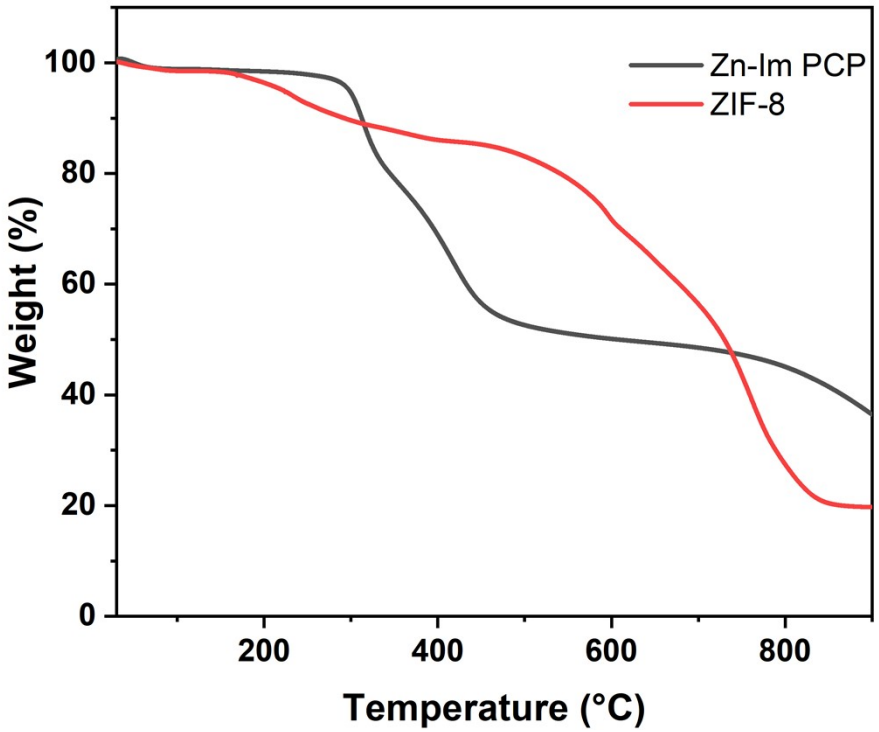

Figure S8. TGA curves of Zn-Im fibers and ZIF-8.

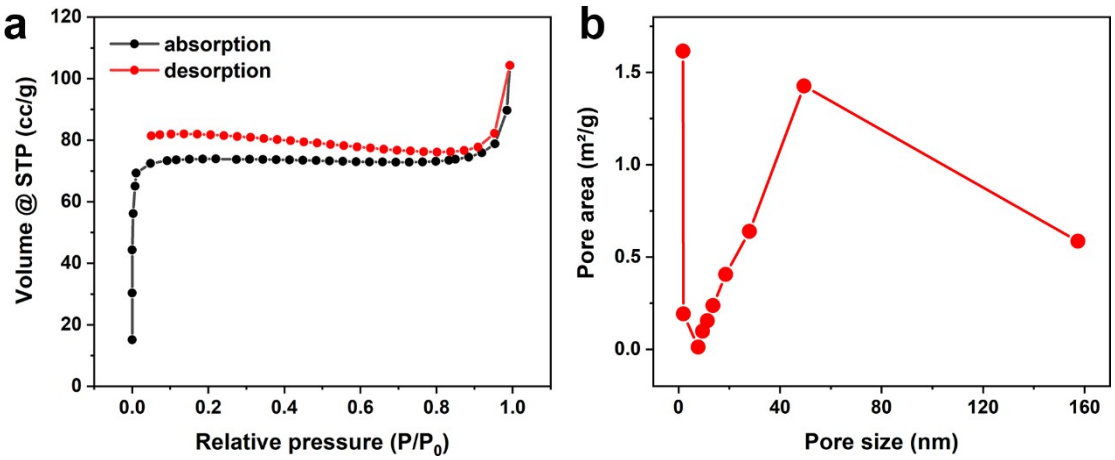

Figure S9. (a) N_2 adsorption and desorption isotherms and (b) pore size distributions for porous carbon fibers after acid leaching.

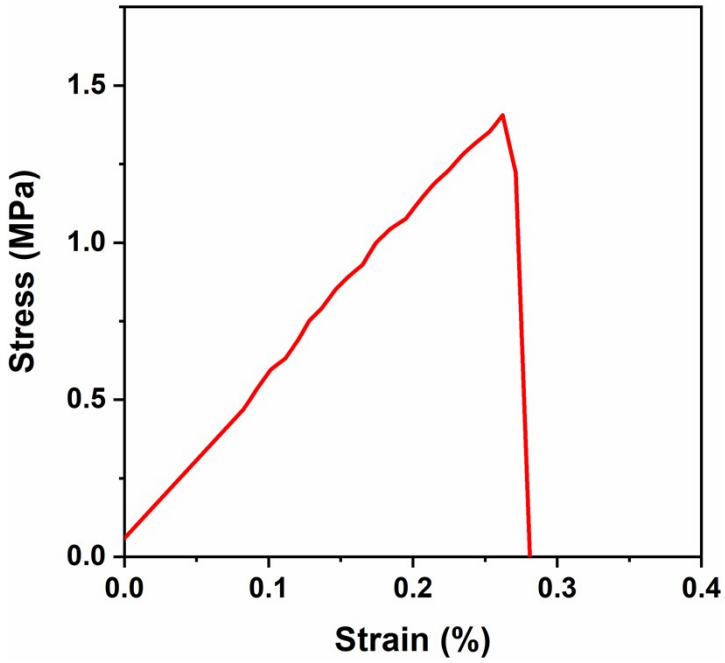

Figure S10. Typical stress-strain curve of porous carbon fibrous membrane.

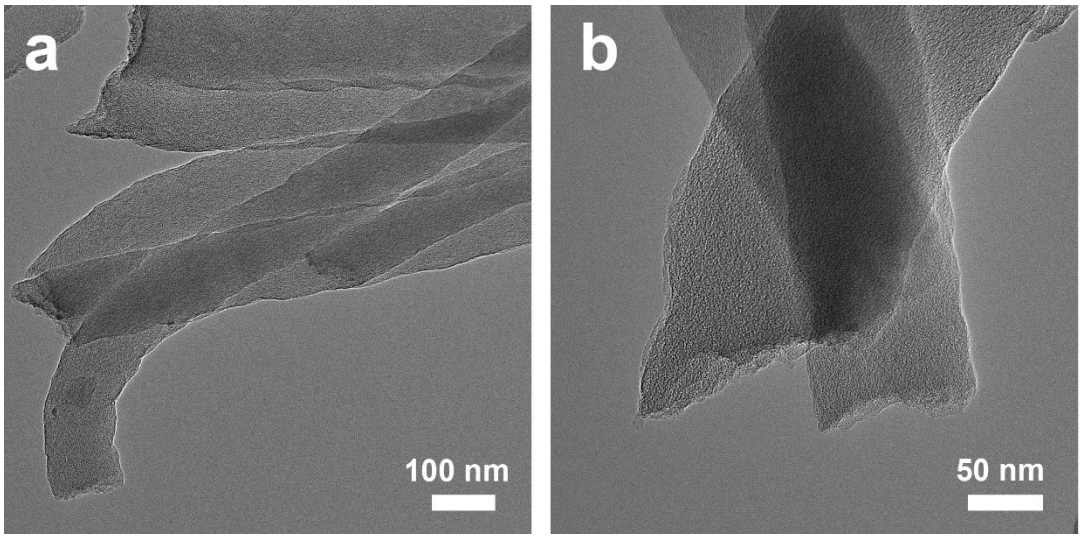

Figure S11. TEM images of Im-Fe-900.

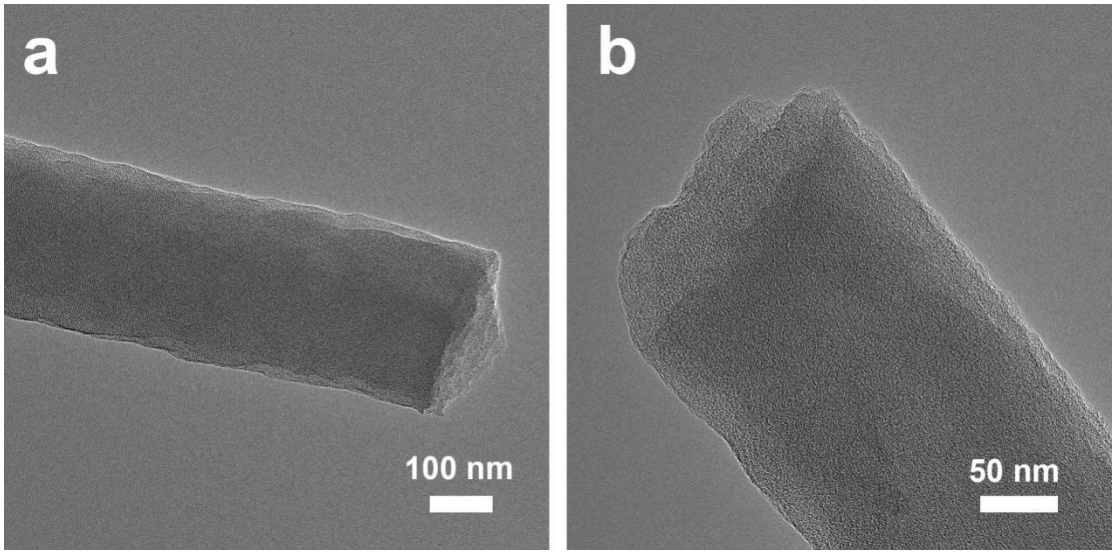

Figure S12. TEM images of Im-Fe-S-900.

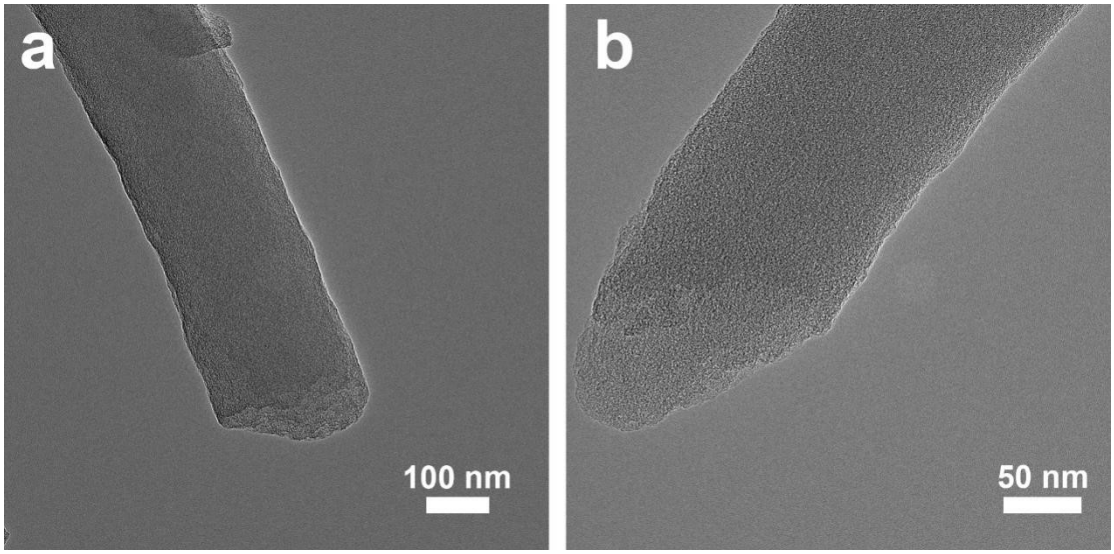

Figure S13. TEM images of Im-Fe-N-900.

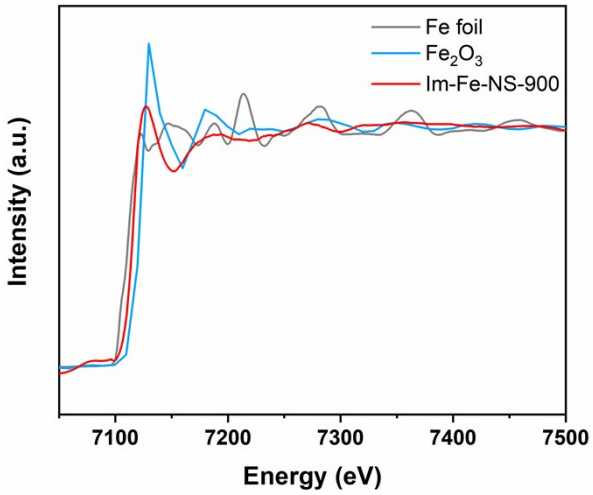

Figure S14. X-ray absorption spectroscopy of Fe foil, Fe_2O_3 and Im-Fe-NS-900

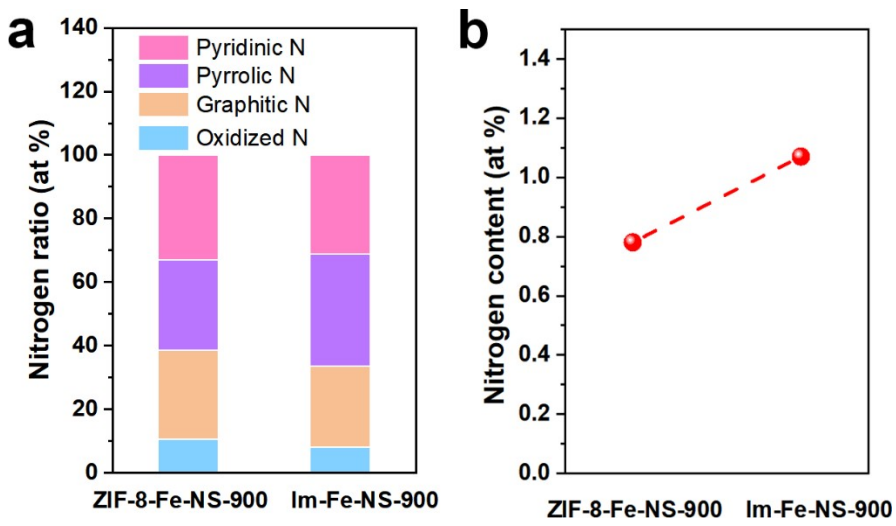

Figure S15. Different N types content of Im-Fe-NS-900 and ZIF-8-Fe-NS-900.

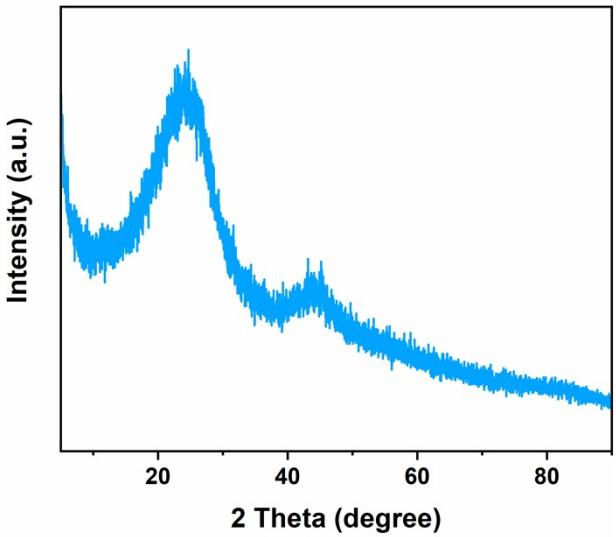

Figure S16. XRD pattern of ZIF-8-Fe-NS-900.

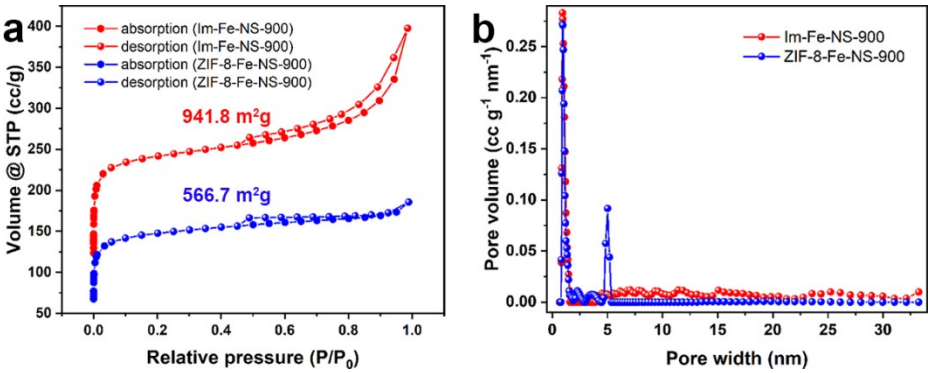

Figure S17. (a) N_2 adsorption and desorption isotherms and (b) pore size distributions for Im-Fe-NS-900 and ZIF-8-Fe-NS-900.

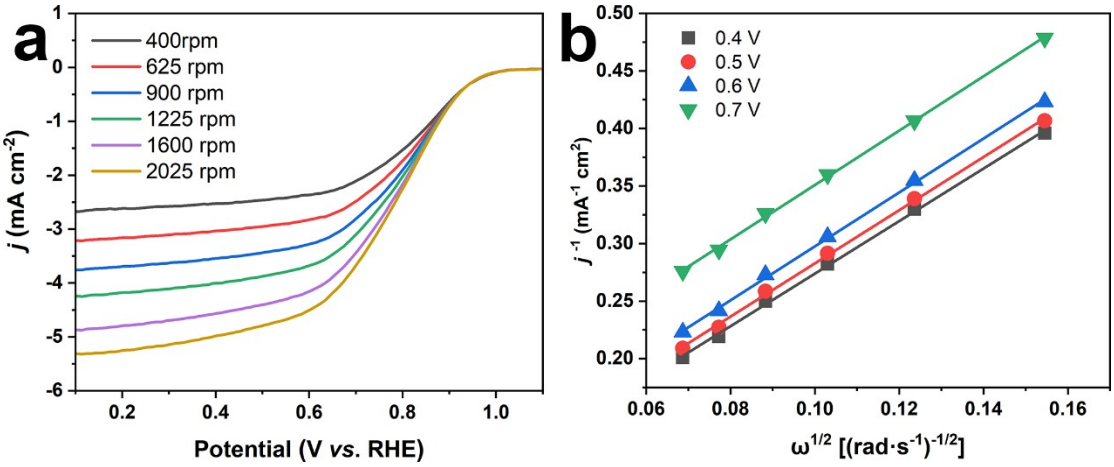

Figure S18. Kinetic-limiting current densities on the Im-Fe-900 catalyst at different rotating speeds.

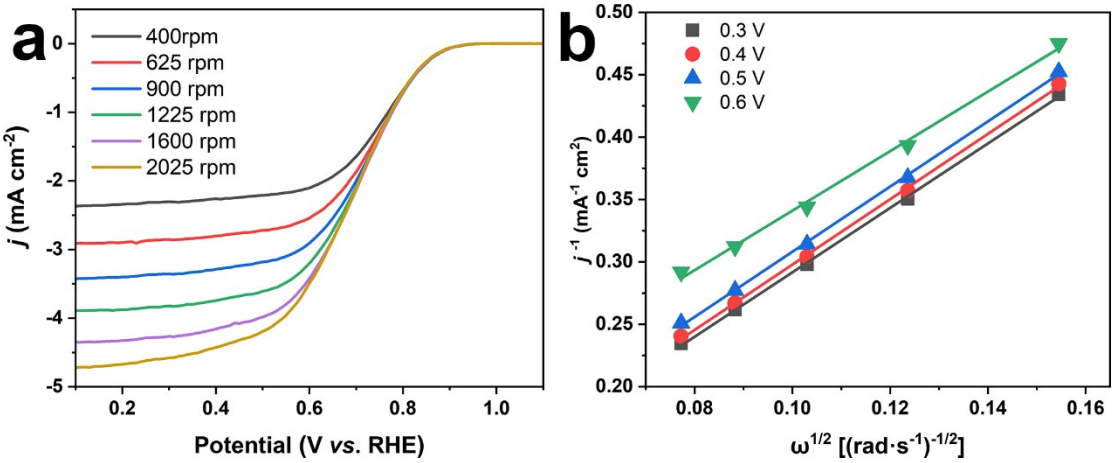

Figure S19. Kinetic-limiting current densities on the Im-Fe-S-900 catalyst at different rotating speeds.

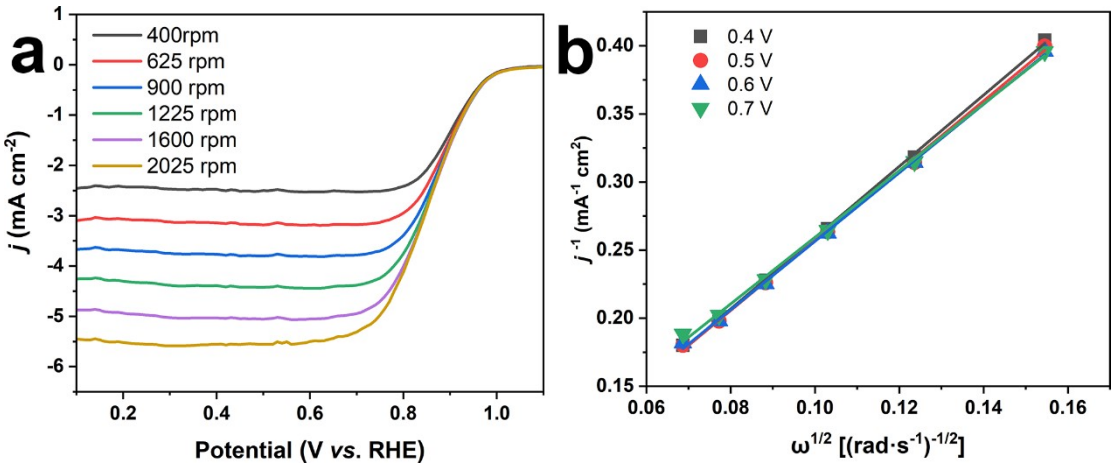

Figure S20. Kinetic-limiting current densities on the Im-Fe-N-900 catalyst at different rotating speeds.

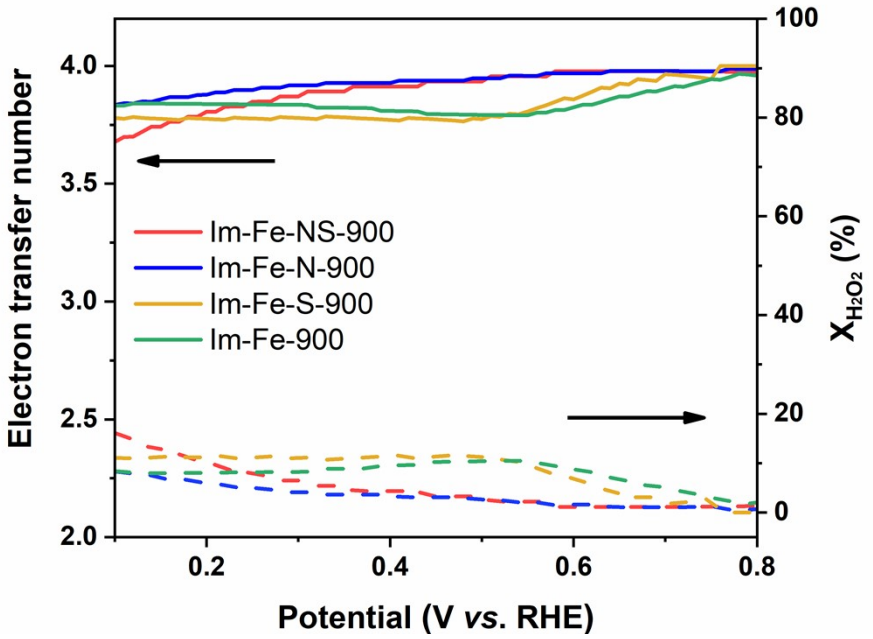

Figure S21. Electron transfer number and H_2O_2 selectivity plots for Im-Fe-900, Im-Fe-S-900, Im-Fe-N-900 and Im-Fe-NS-900.

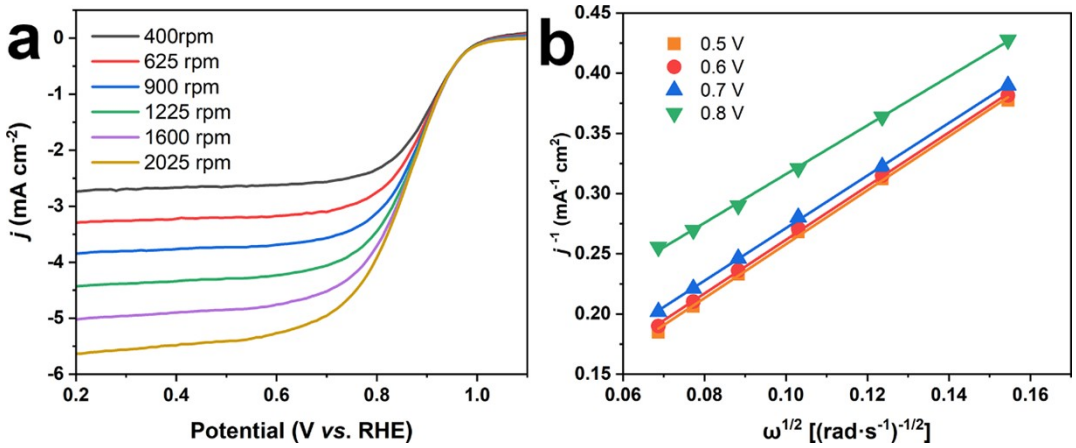

Figure S22. Kinetic-limiting current densities on the ZIF-8-Fe-NS-900 catalyst at different rotating speeds.

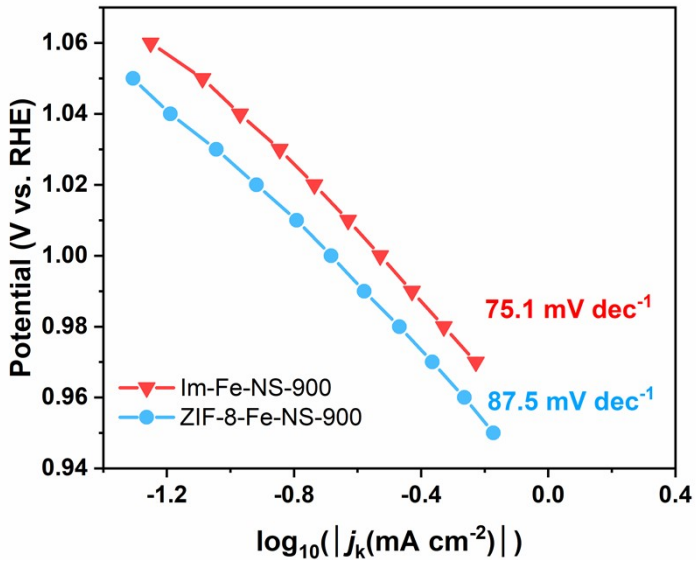

Figure S23. Tafel slope of Im-Fe-NS-900 and ZIF-8-Fe-NS-900.

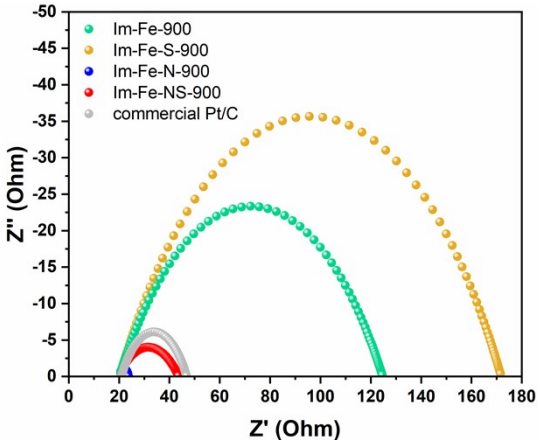

Figure S24. Electrochemical impedance spectra of Im-Fe-900, Im-Fe-S-900, Im-Fe-N-900, Im-Fe-NS-900 and commercial Pt/C.

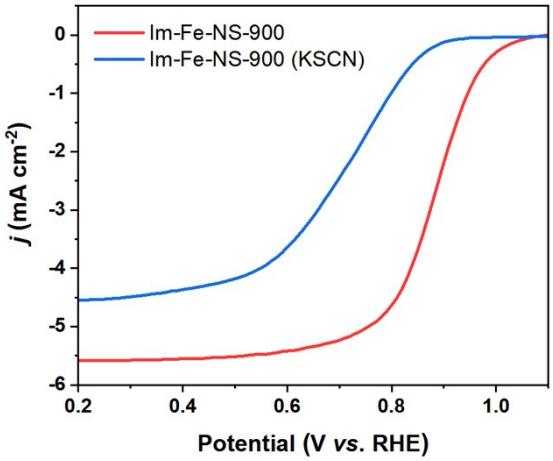

Figure S25. LSV curves of Im-Fe-NS-900 without and with 0.1 M KSCN.

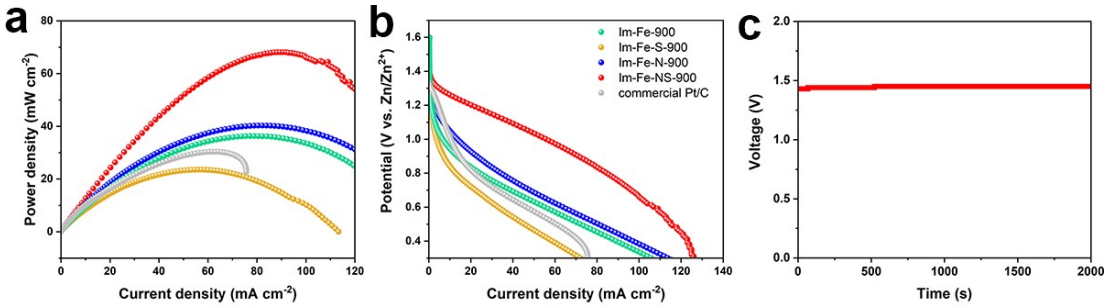

Figure S26. (a) Discharge polarization curves and (b) the corresponding power density plots of Im-Fe-900, Im-Fe-S-900, Im-Fe-N-900, Im-Fe-NS-900-based and Pt/C-based Zn-air battery. (c) Open circuit potential of Im-Fe-NS-900-based Zn-air battery.

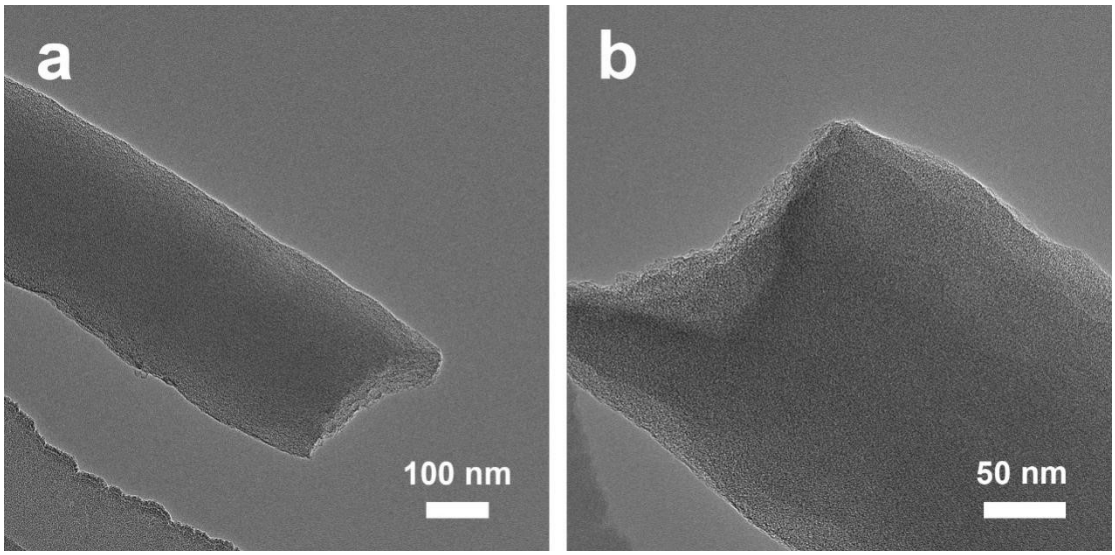

Figure S27. TEM images of Im-Fe-NS-800.

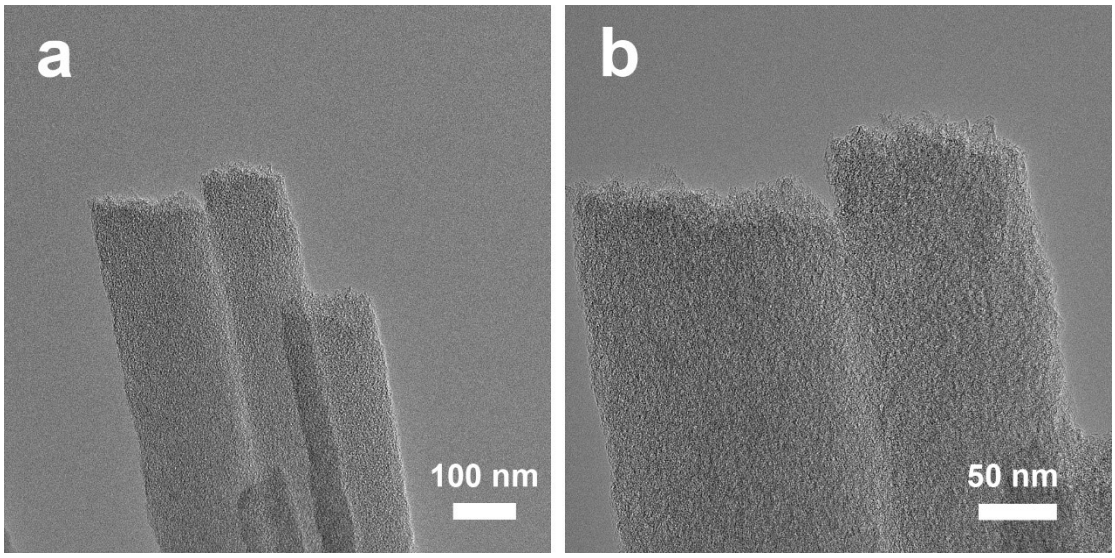

Figure S28. TEM images of Im-Fe-NS-1000.

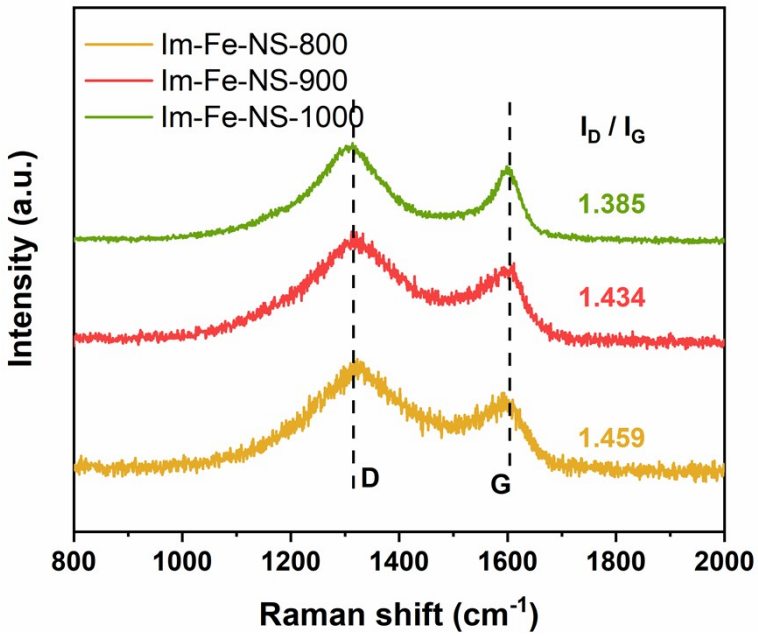

Figure S29. Raman spectra of Im-Fe-NS-800, Im-Fe-NS-900 and Im-Fe-NS-1000.

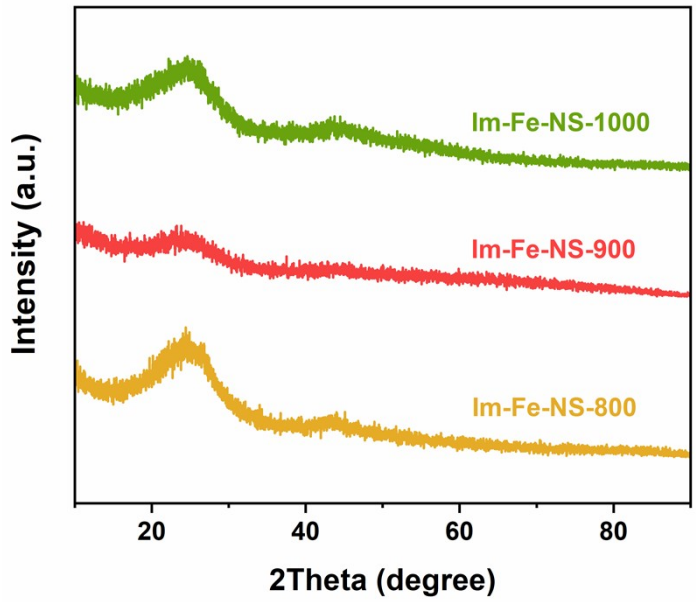

Figure S30. XRD pattern of Im-Fe-NS-800, Im-Fe-NS-900 and Im-Fe-NS-1000.

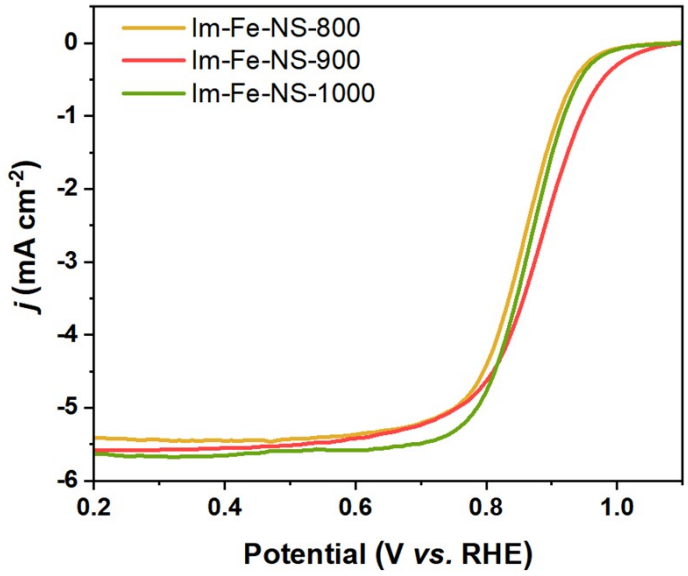

Figure S31. LSV curves of Im-Fe-NS-800, Im-Fe-NS-900 and Im-Fe-NS-1000.

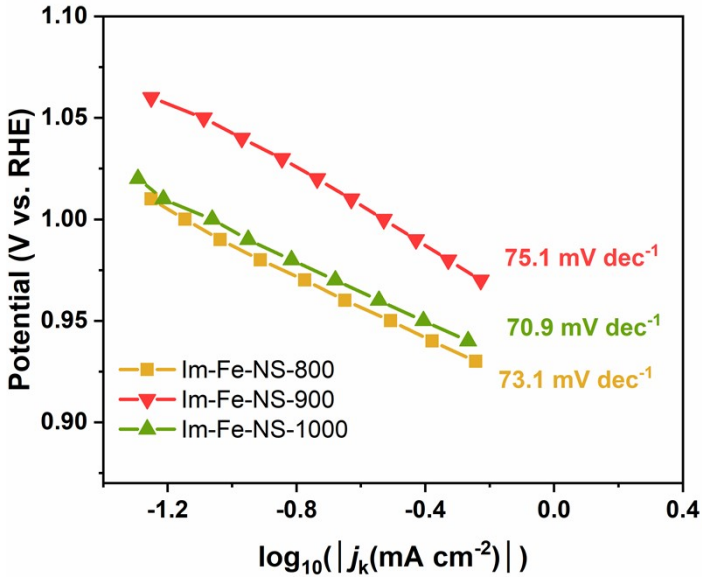

Figure S32. Tafel slope of Im-Fe-NS-800, Im-Fe-NS-900 and Im-Fe-NS-1000.

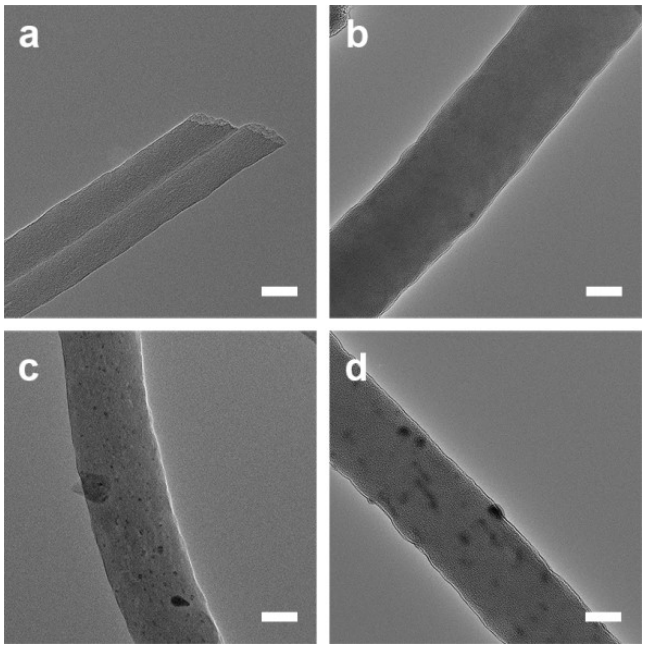

Figure S33. TEM images of Im-Fe-NS-900 ($Fe_{0.25}$), Im-Fe-NS-900 ($Fe_{0.5}$), Im-Fe-NS-900 (Fe_2) and Im-Fe-NS-900 (Fe_4). Scale bar, 100 nm.

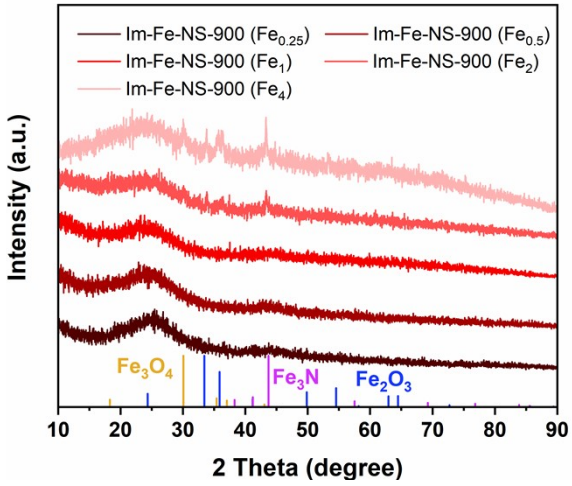

Figure S34. XRD patterns of Im-Fe-NS-900 ($Fe_{0.25}$), Im-Fe-NS-900 ($Fe_{0.5}$), Im-Fe-NS-900 (Fe_1), Im-Fe-NS-900 (Fe_2) and Im-Fe-NS-900 (Fe_4).

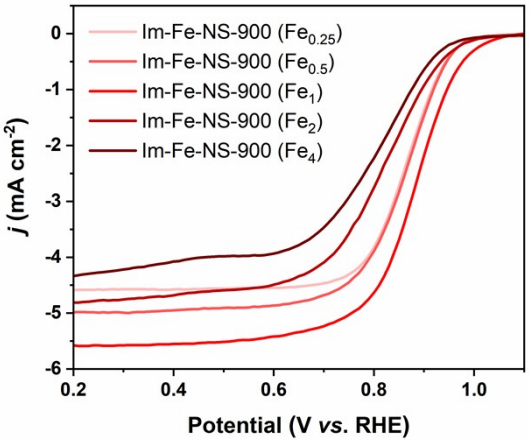

Figure S35. LSV curves of Im-Fe-NS-900 ($Fe_{0.25}$), Im-Fe-NS-900 ($Fe_{0.5}$), Im-Fe-NS-900 (Fe_1), Im-Fe-NS-900 (Fe_2) and Im-Fe-NS-900 (Fe_4).

3. Supporting Tables

Table S1. The ORR activity of recent reported Fe-N_4 catalysts in the basic condition.

Materials	$E_{1/2}$	E_{onset}	Reference
Im-Fe-NS-900	**0.89**	**1.04**	***This work***
Fe-COF-900	0.81	0.92	1
Fe-N-GDY	0.89	1.05	2
Fe/OES	0.85	1.00	3
SA-250Fe/NPC-800	0.85	0.97	4
Fe-N/S-C	0.882	0.97	5
Fe–N/C-700	0.863	0.983	6
FeNi SAs/NC	0.84	0.98	7
Fe-AC-2	0.84	0.98	8

Table S2. The N content of prepared catalysts.

Materials	Total N content	Pyrrolic N content	Pyridinic N content	Graphitic N content	Oxidized N Content
Im-Fe-900	2.44 at%	0.53 at%	0.85 at%	0.84 at%	0.22 at%
Im-Fe-N-900	3.19 at%	0.98 at%	0.82 at%	0.95 at%	0.44 at%
Im-Fe-S-900	4.19 at%	0.75 at%	1.51 at%	1.43 at%	0.50 at%
Im-Fe-NS-900	3.04 at%	1.07 at%	0.95 at%	0.77 at%	0.25 at%

Table S3. The metal content of samples measured by ICP.

Materials	Metal species	Content (wt%)
Porous carbon fibers	Zn	2.28
Porous carbon fibers after acidic leaching	Zn	0.03
Im-Fe-NS-900	Fe	0.56
	Zn	0.01

4. Reference

1. S. Yang, X. Li, T. Tan, J. Mao, Q. Xu, M. Liu, Q. Miao, B. Mei, P. Qiao, S. Gu, F. Sun, J. Ma, G. Zeng, Z. Jiang, *Appl. Catal.- B* **2022,** *307,* 121147.
2. M. Li, Q. Lv, W. Si, Z. Hou, C. Huang, *Angew. Chem. Int.* Ed. **2022,** e202208238.
3. C.-C. Hou, L. Zou, L. Sun, K. Zhang, Z. Liu, Y. Li, C. Li, R. Zou, J. Yu, Q. Xu, *Angew. Chem. Int. Ed.* **2020,** *59,* 7384-7389.
4. J.-S. Jiang, H.-L. Wei, A.-D. Tan, R. Si, W.-D. Zhang, Y.-X. Yu, *Chin. J. Catal.* **2021,** *42,* 753-761.
5. L. Li, S. Huang, R. Cao, K. Yuan, C. Lu, B. Huang, X. Tang, T. Hu, X. Zhuang, Y. Chen, *Small* **2022,** *18,* 2105387.
6. Z. K. Yang, C.-Z. Yuan, A.-W. Xu, *Nanoscale* **2018,** *10,* 16145-16152.
7. D. Yu, Y. Ma, F. Hu, C.-C. Lin, L. Li, H.-Y. Chen, X. Han, S. Peng, *Adv. Energy Mater.* **2021,** *11,* 2101242.
8. Y. Wang, Q. Li, L.-C. Zhang, Y. Wu, H. Chen, T. Li, M. Xu, S.-J. Bao, *J. Mater. Chem. A* **2021,** *9,* 7137-7142.